ELSEVIER

Contents lists available at ScienceDirect

Experimental Thermal and Fluid Science

journal homepage: www.elsevier.com/locate/etfs



Microscale two-dimensional (2D) temperature mapping by ratiometric fluorescence imaging under orthogonal excitations



Chen Chen, Tong Shen, Zhidong Du, Junxue Zhang, Jicheng Wang, Amy Marconnet, Liang Pan*

School of Mechanical Engineering & Birck Nanotechnology Center, Purdue University, West Lafayette, IN 47907, USA

ARTICLE INFO

Keywords: Temperature mapping Ratiometric thermometry Fluorescence imaging Fluorescence anisotropy

ABSTRACT

Microscale temperature mapping in liquids is of great importance in many areas of research such as microfluidics and biology. Among the current thermometric approaches, optical probing using fluorescence is particularly desirable because of its high spatial resolution and non-invasive nature. Here we report a new microscale two-dimensional (2D) fluorescence thermometry. This method exploits the temperature dependence of rotational molecular motion and its influence on the depolarization of fluorescence light, by measuring the difference in fluorescence intensities excited by orthogonal polarizations. With one charge coupled device (CCD) camera, we get 2D ratiometric mappings of temperature from successively recorded fluorescence images under alternatively polarized excitations. We demonstrate reliable temperature mapping in liquids at sub-1 °C temperature accuracy and sub-10 μ m spatial resolution. We also show that the proposed thermometry approach is robust against fluorescence intensity variations, suitable for 2D mapping and of fast readout that is comparable to CCD framerate. Moreover, it is easy to be integrated into microscope systems since only rotation of excitation polarization is needed.

1. Introduction

Temperature mapping in liquids is of fundamental importance in many areas, such as applications to locate thermal hotspots in microfluidics and in biological thermogenesis processes [1-11]. Fluorescence-based thermometry is of particular interest due to its non-contact and non-invasive advantages [6-22]. Among those methods, fluorescence anisotropy measurement has been successfully implemented in many applications because of its reliable temperature dependence, high spatial resolution and fast readout rate [7,8,13,22-24]. Most of these works use illumination by a linearly polarized light as excitation and capture the emission inequality along two different polarization directions. Here temperature plays an important role since a photo-excited molecule may rotate over a substantial angle before emitting light due to Brownian motion at a high temperature, which randomizes the polarization in fluorescence emission. This effect is known as the temperature-induced fluorescence depolarization. The higher the temperature is, the stronger the effect becomes. Thus a fluorescent molecule can be utilized as a thermal probe for the local environment. By measuring the fluorescent emission of two orthogonal polarizations, an intensity-independent ratio can be obtained to extract temperature information. Due to the ratiometric character, this polarization based anisotropy thermometry is robust against temporal fluctuation caused

by photobleaching and spatial non-uniformity of fluorescence intensities, making it desirable in many applications [6,7,15]. Besides polarization, the emission inequality along different directions offers another degree of freedom for anisotropy measurement, which has been recently demonstrated [13]. Instead of measuring two orthogonal polarizations, the directionality based method resolves angular distribution of fluorescence emission using two distinct numerical apertures, which essentially are two different angular collecting cones. Since the detected angular distribution is less affected by polarizing environments compared to polarization, the directionality based anisotropy method is intrinsically more applicable to polarizing materials, such as a solution containing metal nanoparticles of diameters around several nanometers which is commonly used as fluorescent labeler in superresolution microscopy, while inheriting the advantages of other ratiometric temperature mapping methods. Here, we experimentally demonstrate that using two successive excitations of orthogonal polarizations, reliable mapping of temperature can be achieved in liquids at sub-1 °C temperature accuracy and sub-10 µm spatial resolution by measuring directionality based anisotropy with one charge coupled device (CCD). This new thermometry shares the same advantages claimed for fluorescent anisotropy based methods, including robustness against intensity variations caused by photobleaching, suitability for two-dimensional (2D) imaging and readout rate as fast as the framerate

E-mail address: liangpan@purdue.edu (L. Pan).

^{*} Corresponding author.

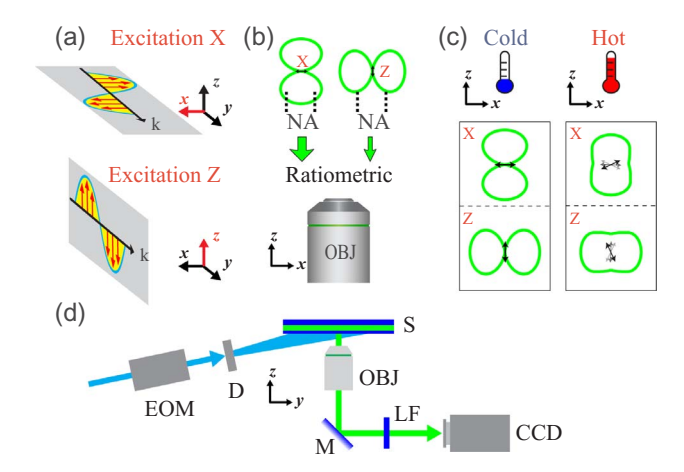


Fig. 1. Working principle of the thermometry. (a) x-polarized excitation beam and z-polarized excitation beam. (b) The green contours show the cross-sectional intensity distributions of fluorescence emission in different directions when the polarized fluorescence molecules are along x and z respectively. Strongest emission occurs along the direction perpendicular to the molecule polarization. Different amounts of fluorescence emission can enter an objective lens of a finite numerical aperture (NA) for x- and z-polarized fluorescence molecules. (c) Comparison between cold and hot cases: the intensity difference between two excitations is less distinguishable under a higher temperature. (d) Schematic of optical setup: dark-field illumination is modulated by an electro-optical modulator (EOM) through a diffuser (D); in the sample (S), fluorescence solution is sandwiched by a slide and a coverslip; fluorescence is collected by a microscope objective (OBJ) and then directed into a charge-coupled device (CCD) camera after a long-pass filter (LF) with a cutoff below 500 nm. (For interpretation of the references to colour in this figure legend, the reader is referred to the web version of this article.)

of the used detector. It also simplifies the detection scheme in traditional anisotropy measurements since no extra modification in detection path is required. Thus it can be easily integrated into fluorescence microscopy systems by alternating polarizations on the excitation side and provide additional thermal information (temperature, viscosity, ...) together with the common optical information.

2. Working principle

Fig. 1 illustrates the working principle of the newly proposed thermometry method. A fluorescent molecule is excited using a beam of linearly polarized light and a non-isotropic angular distribution in emission is expected from its induced transition dipole. For a system at a low temperature, we can approximately have: (i) the induced transition dipole has a constant magnitude and is parallel to the polarization direction of the excitation light; and (ii) the transition dipole does not rotate away substantially from its original direction before emitting fluorescence. Under these approximations, the emission directions of the transition dipole are primarily parallel to the y-z plane when the molecule is excited by an x-polarized light and to the x-y plane for a zpolarized light (Fig. 1(a) and (b)). The green contours in Fig. 1(b) shows the cross-sectional intensity distributions of fluorescence emission in different directions when the polarized fluorescence molecules are along x and z respectively. The emissions from these assemblies of fluorescence molecules both have the doughnut-like emission patterns similar as those of dipole emitters. Strongest emission occurs along the directions perpendicular to the dipole. When collecting the emission along z direction using an objective lens of a finite numerical aperture (NA), the two configurations would give the maximum and minimum fluorescent intensities respectively, which corresponds to the highest fluorescent emission anisotropy. As for the first approximation, it is true for an ensemble of fluorescent molecules in a statistical sense which also applies in this work [7,8,13,25]. The second approximation is also valid when the local temperature is low, meaning thermal rotation is not significant during the lifetime of the photo-excited molecules. As the temperature increases, the molecules quickly rotate away from their original orientations and the emission anisotropy along different directions starts to smooth out until the objective cannot accurately distinguish two configurations apart at a certain high temperature (Fig. 1(c)). In this way, the temperature information can be extracted based on the difference between two fluorescence intensities using orthogonal excitations. Here we can see that the thermometry approach based on this working principle is an indirect measurement of liquid temperature. Temperature changes local viscosity of the liquid and the change of viscosity in turn alters the rotation of the fluorescent molecules.

To quantitatively correlate temperature with the difference between two fluorescence intensities under orthogonal excitations, we define a ratiometric parameter S, named "sameness of two excitations in emission", as $S \equiv S_0 + (I_z - I_x)/I_x$, where I_x and I_z are the collected fluorescence intensities by the objective lens given the excitations are polarized along x and z directions, respectively. And S_0 is a reference point to be calibrated out at a known reference temperature. Note that S increases as temperature increases and anisotropy deceases. We call S "sameness" for short hereafter. Assuming the lifetime of fluorescence is T_F , the collected fluorescence intensity can be calculated as [13]

$$I = C \tau_F \left[-a \frac{(3\cos^2 \theta_e - 1)}{2} \frac{1}{1 + \tau_F / \tau_R} + b \right]$$
 (1)

where C is a factor roughly equal to the total number of fluorescent molecules whose fluorescence can be collected by the objective lens and is related to the local concentration of fluorescent molecules and the thickness of the solution, a and b are two positive constants accounting for collecting efficiencies of fluorescence components along different directions and are related to the angular distribution of fluorescent emission and the numerical aperture of the collecting objective lens, θ_e is the polarization angle of the excitation light with respect to z axis, and τ_R is the rotational correlation time, a characteristic time to quantify how fast the molecules rotate in liquids. The term $(3\cos^2\theta_e-1)/2$ comes from the average of photoselection effect when an ensemble of fluorescent molecules gets excited by a linearly polarized light. Here we assume all the parameters above except for τ_R are temperature independent [7,8,13] for simplicity. Then S can be expressed as $S = S_0 + 1/[(a/6b)f(T) + 1/3] - 3$, where $f(T) \equiv 1/(1 + \tau_F/\tau_R)$ directly related to temperature. By choosing a reference temperature T_0 at which S equals zero, we have

$$S = \frac{1}{p_0 f(T) + 1/3} - \frac{1}{p_0 f(T_0) + 1/3}$$
 (2)

where a/6b is replaced by another constant p_0 .

3. Calibration

Fig. 2(a) shows the calibration of sameness as a function of temperature. The calibration was performed by uniformly heating up the sample to a specific temperature with a thermoelectric cooler (Thorlabs TEC 3-6) controlled by a temperature controller (Thorlabs TED200C) together with a temperature transducer (Thorlabs AD590). The TEC and the temperature transducer were attached to two opposite sides of the sample in which the fluorescence solution was sandwiched by a slide and a coverslip. Every time after temperature stabilizes, the corresponding sameness of two excitations in emission was calculated using the averaged fluorescence intensities recorded by our EMCCD (Cascade 1K). The error bars correspond to the standard deviation in each measurement. A relatively larger error bar at a higher temperature is caused by reduced fluorescence intensities, which is common in fluorescence thermometries [8,13,26]. As temperature becomes significantly higher, our experimental data suggest that the loss in florescence has strong effect on the measuring sensitivities, which requires to increase exposure time accordingly. The theoretical trend in Fig. 2(a) is the best fit of Eq. (2) in the least-squares sense by allowing the glycerol volume

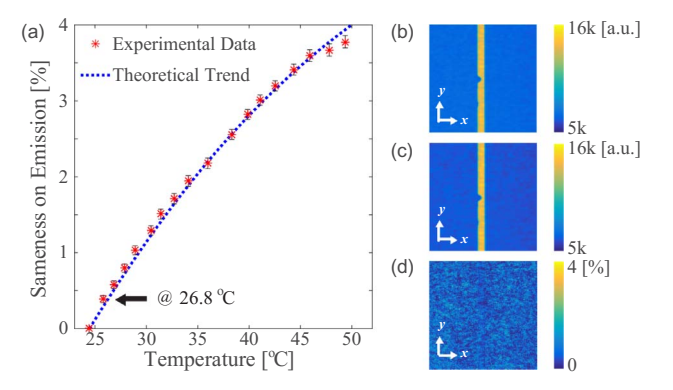


Fig. 2. Temperature calibration. (a) Calibrated sameness S as a function of temperature. (b) Fluorescence intensity map with x-polarized excitation at a uniform temperature 26.8 °C. (c) Fluorescence intensity map with z-polarized excitation at a uniform temperature 26.8 °C. (d) Calculated map of sameness based on panels b and c. The size of all the maps is 400 μ m \times 400 μ m unless otherwise stated.

fraction and p_0 to vary. The best fit is obtained for a glycerol volume fraction of 0.7 with p_0 equal to 0.0188. Other used parameters are $\tau_F = 3.7 \text{ ns}, V = 0.47 \text{ nm}^3, T_0 = 24.4 \text{ °C} \text{ and } \tau_R = V \nu(T)/k_B T, \text{ where } \nu(T)$ is dynamic viscosity calculated by an empirical formula for glycerolwater mixture with a certain glycerol volume fraction [27] and k_B is the Boltzmann constant. The theoretical curve agrees well with the experimental data, suggesting the defined parameter of interest S given by Eq. (2) is a good temperature indicator. Also, the term *C* in Eq. (1) does not appear in Eq. (2), indicating that the factors equally affecting fluorescence intensities of two excitation polarizations, such as variations in fluorescence molecule concentration, have little effect on the sameness. This is verified in our experiment, as shown in Fig. 2(b)-(d). Fig. 2(b) is the fluorescence intensity map of about 10 μm thick solution (fluorescein concentration about 10^{-4} M) recorded by the EMCCD under x-polarized excitation of 450 nm laser light using a dark-field illumination setup [13] with a 20X objective lens (Mitutoyo Plan Apo NUV). The EMCCD is directly connected to one bottom port of a Nikon inverted microscope (Eclipse Ti-U model) in a conventional scheme of fluorescence microscopy, as shown in Fig. 1(d). The detailed information of used optical components can be found in our previous work [13]. The field of view is $400 \, \mu m \times 400 \, \mu m$ on the object side. The bright stripe corresponds to an aluminum heater fabricated on the supporting microscope slide using photolithography [13,28]. The width of the heater is measured to be 24 µm. A notch about half the width of the heater is intentionally made to generate a non-uniform 2D temperature field with a hotspot. The collected fluorescence intensity on the heater is about two times larger compared to that of the surrounding slide area because of the reflection of fluorescence. The nonuniformity in small domains of the intensity map, which is more visible in its counterpart of z-polarized excitation in Fig. 2(c), is caused by laser speckles since a random phase diffuser (Optotune LSR-3005-6D-VIS) is introduced in the excitation beam path to reduce interference effect of laser light. Fig. 2(d) shows the calculated map of sameness at 26.8 °C based on two maps of intensity in Fig. 2(b) and (c). It can be seen that both the heater and slide parts have the same average of S, despite of the reflections of fluorescence due to the aluminum heater and fluctuations in excitation because of the laser speckles. This enables us to use a universal calibration curve for all the areas with a temperature resolution better than 1 °C.

4. Results and discussion

To demonstrate the ability of 2D mapping of this new thermometry, we used the heater to generate a non-uniform temperature distribution [13] inside the same solution used for calibration. During each exposure time of 500 ms for the CCD frame, ten current pulses of the same

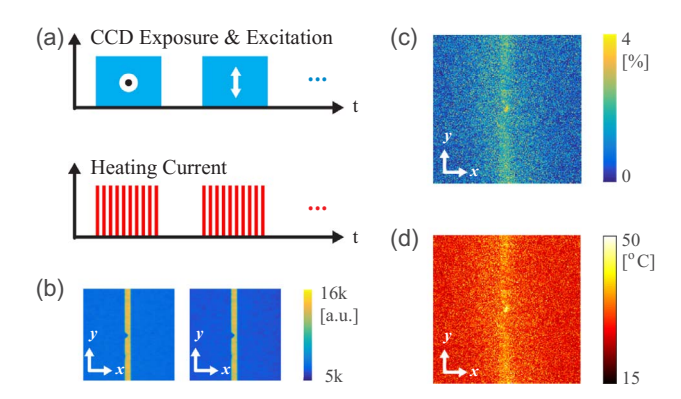


Fig. 3. Mapping of 2D temperature distribution. (a) Time sequences of CCD exposure and electric heating current. (b) Fluorescence intensity maps corresponding to orthogonal polarizations of excitation in panel a. (c) Calculated map of sameness. (d) Map of temperature corresponding to panel c.

amplitude 42 mA were periodically applied through the heater with each duration time of 35 ms, as illustrated in Fig. 3(a). To reduce the fluorescence photo-bleaching, the laser excitation was only turned on when the CCD was under exposure. Between two successive frames which were separated by a time interval of 850 ms, the polarization of laser excitation with an extinction ratio of about 50 was alternated using an electro-optic modulator (EOM) (Conoptics 350-160). Instead of using EOM to dynamically modulate the polarization of one beam, two separate beams with orthogonal polarizations, which may be of different colors, can also be used when the timing is properly controlled. Fig. 3(b) shows two adjacent frames when heating current is present, aligned with the time sequences in Fig. 3(a). Based on the two intensity images, the corresponding S map can be calculated with a pixel binning factor of four, as shown in Fig. 3(c). Applying the calibration curve in Fig. 2(a) to Fig. 3(c), the temperature distribution in Fig. 3(d) is obtained. A thermal hotspot near the position of the heater notch can be clearly seen due to the increase of local resistivity of the heater line. This result demonstrates that a 2D temperature distribution can be obtained at a readout rate comparable to the framerate of the CCD using this new ratiometric temperature mapping method. The random noise in Fig. 3(d) is mainly caused by random laser speckles and can be further reduced by repeating the same measurement several times or using an incoherent light source. In principle, the temporal resolution of this thermometry can be extended to tens of nanoseconds, which is limited by the rotational correlation time and the lifetime of the used fluorescent molecules. One possible scheme is recently demonstrated by Glorieux's group [29] where they excited the fluorescence using a laser pulse of nanosecond time duration after a tunable time delay with nanosecond temporal resolution after the thermal excitation, known as a stroboscopic approach.

Fig. 4(a) shows a temperature map that was obtained by averaging four temperature mappings under the same condition. Both the thermal hotspot and the general trend of the heater are clearly visible. To have a better understanding of our system, we perform a multiphysics simulation in COMSOL software using a similar configuration in our previous model [13]. Our measured temperature distribution agrees well with the numerical estimation as shown in Fig. 4(b) and (c), where Fig. 4(b) is the simulated 2D temperature map using a simulation current of 55 mA and Fig. 4(c) is the experimental and simulated temperature profiles by averaging along y direction of temperature maps. The effective thickness of the heater is 80 nm. In our numerical model, the thermal conductivity of the glycerol-water mixture is taken as 0.38 W/(m·K), a reasonable value between those of glycerol and water [30]. All the values of other physical parameters, including densities, volumetric heat capacities and thermal conductivities, are commonly used ones. In the simulation of a single current pulse, temperature around the heater does not recover to room temperature at the

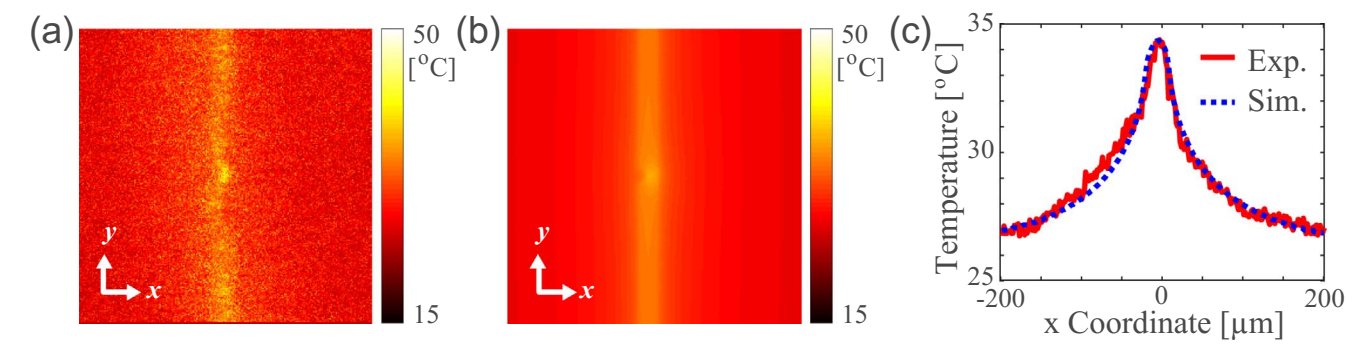


Fig. 4. Comparison between experiment and simulation. (a) Temperature map in experiment, average of four successive measurements. (b) Temperature map in simulation. (c) Temperature profiles along x direction by averaging the y direction of the temperature maps in panels a and b.

end of 50 ms after applying the heating current during the first 35 ms. This thermal accumulation effect is taken into account by providing the measured background temperature as the ambient solution temperature, which is 3 °C higher than the room temperature.

5. Conclusion

To summarize, we have demonstrated the plausibility of rotating the polarizations on the excitation side to perform fluorescence anisotropy measurement, which is based on the directionality in emission. Using one CCD, we measured the 2D temperature distribution in liquids generated by a metallic film heater with a temperature resolution better than 1 °C and verified the advantages of ratiometric measurements, such as stability with respect to intensity variation, suitability of 2D mapping and rapidity in readout rate. Since the dark-filed illumination scheme is compatible with total internal reflection fluorescence (TIRF) microscopy, we expect that our new thermometry can be integrated into widely used fluorescence microscopy and can offer additional thermal information besides traditional optical fluorescence measurements.

Acknowledgements

We acknowledge the financial support from National Science Foundation (NSF) (CMMI-1405078, CMMI-1554189, CMMI-1634832) and Purdue Research Foundation (PRF).

References

- [1] F. Menges, P. Mensch, H. Schmid, H. Riel, A. Stemmer, B. Gotsmann, Temperature mapping of operating nanoscale devices by scanning probe thermometry, Nat. Commun. 7 (2016) 10874.
- [2] M. Mecklenburg, W.A. Hubbard, E.R. White, R. Dhall, S.B. Cronin, S. Aloni, B.C. Regan, Nanoscale temperature mapping in operating microelectronic devices, Science 347 (2015) 629–633.
- [3] M.M. Kim, A. Giry, M. Mastiani, G.O. Rodrigues, A. Reis, P. Mandin, Microscale thermometry: a review, Microelectron. Eng. 148 (2015) 129–142.
- [4] C.B. Saltonstall, J. Serrano, P.M. Norris, P.E. Hopkins, T.E. Beechem, Single element Raman thermometry, Rev. Sci. Instrum. 84 (2013) 064903.
- [5] Y. Yue, X. Wang, Nanoscale thermal probing, Nano Rev. 3 (2012) 11586.
- [6] K. Okabe, N. Inada, C. Gota, Y. Harada, T. Funatsu, S. Uchiyama, Intracellular temperature mapping with a fluorescent polymeric thermometer and fluorescence lifetime imaging microscopy, Nat. Commun. 3 (2012) 705.
- [7] J.S. Donner, S.A. Thompson, M.P. Kreuzer, G. Baffou, R. Quidant, Mapping intracellular temperature using green fluorescent protein, Nano Lett. 12 (2012) 2107–2111.
- [8] G. Baffou, M.P. Kreuzer, F. Kulzer, R. Quidant, Temperature mapping near plasmonic nanostructures using fluorescence polarization anisotropy, Opt. Express 17 (2009) 3291–3298.

- [9] M. Farzaneh, K. Maize, D. Lüerßen, J.A. Summers, P.M. Mayer, P.E. Raad, K.P. Pipe, A. Shakouri, R.J. Ram, J.A. Hudgings, CCD-based thermoreflectance microscopy: principles and applications, J. Phys. D: Appl. Phys. 42 (2009) 143001.
- [10] J.M. Son, J.H. Lee, J. Kim, Y.H. Cho, Temperature distribution measurement of Au micro-heater in microfluidic channel using IR microscope, Int. J. Precis. Eng. Man. 16 (2015) 367–372.
- [11] H.F. Arata, P. Low, K. Ishizuka, C. Bergaud, B. Kim, H. Noji, H. Fujita, Temperature distribution measurement on microfabricated thermodevice for single biomolecular observation using fluorescent dye, Sens. Actuator B-Chem. 117 (2006) 339–345.
- [12] P. Löw, B. Kim, N. Takama, C. Bergaud, High-spatial-resolution surface-temperature mapping using fluorescent thermometry, Small 4 (2008) 908–914.
- [13] C. Chen, Z. Du, J. Wang, L. Pan, Temperature mapping using molecular diffusion based fluorescence thermometry via simultaneous imaging of two numerical apertures, Opt. Express 24 (2016) 26599–26611.
- [14] D.M. Toyli, C.F. de las Casas, D.J. Christle, V.V. Dobrovitski, D.D. Awschalom, C.F. De, D. David, Fluorescence thermometry enhanced by the quantum coherence of single spins in diamond, Proc. Natl. Acad. Sci. U.S.A. 110 (2013) 8417–8421.
- [15] L. Gao, C. Zhang, C.Y. Li, L.H.V. Wang, Intracellular temperature mapping with fluorescence-assisted photoacoustic-thermometry, Appl. Phys. Lett. 102 (2013) 193705
- [16] M.Y. Berezin, S. Achilefu, Fluorescence lifetime measurements and biological imaging, Chem. Rev. 110 (2010) 2641–2684.
- [17] Y. Zhuang, Q. Xu, F. Huang, P. Gao, Z. Zhao, X. Lou, F. Xia, Ratiometric fluorescent bioprobe for highly reproducible detection of telomerase in bloody urines of bladder cancer patients, ACS Sens. 1 (2016) 572–578.
- [18] C. Li, Y. Yue, Fluorescence spectroscopy of graphene quantum dots: temperature effect at different excitation wavelengths, Nanotechnology 25 (2014) 435703.
- [19] J. Wu, T.Y. Kwok, X. Li, W. Cao, Y. Wang, J. Huang, Y. Hong, D. Zhang, W. Wen, Mapping three-dimensional temperature in microfluidic chip, Sci. Rep. 3 (2013)
- [20] G.A. Robinson, R.P. Lucht, N.M. Laurendeau, Two-color planar laser-induced fluorescence thermometry in aqueous solutions, Appl. Opt. 47 (2008) 2852–2858.
- [21] K.F. Schrum, A.M. Williams, S.A. Haerther, D. Benamotz, Molecular fluorescence thermometry, Anal. Chem. 66 (1994) 2788–2790.
- [22] R. Zondervan, F. Kulzer, H. van der Meer, J.A.J.M. Disselhorst, M. Orrit, Laser-driven microsecond temperature cycles analyzed by fluorescence polarization microscopy, Biophys. J. 90 (2006) 2958–2969.
- [23] A. Kawski, Fluorescence anisotropy: Theory and applications of rotational depolarization, Crit. Rev. Anal. Chem. 23 (1993) 459–529.
- [24] G. Baffou, C. Girard, R. Quidant, Mapping heat origin in plasmonic structures, Phys. Rev. Lett. 104 (2010) 136805.
- [25] A. Penzkofer, J. Wiedmann, Orientation of transition dipole moments of Rhodamine 6G determined by excited state absorption, Opt. Commun. 35 (1980) 81–86.
- [26] R. Zondervan, F. Kulzer, M.A. Kol'chenk, M. Orrit, Photobleaching of Rhodamine 6G in poly(vinyl alcohol) at the ensemble and single-molecule levels, J. Phys. Chem. A 108 (2004) 1657–1665.
- [27] N.S. Cheng, Formula for the viscosity of a glycerol-water mixture, Ind. Eng. Chem. Res. 47 (2008) 3285–3288.
- [28] W. Srituravanich, L. Pan, Y. Wang, C. Sun, D.B. Bogy, X. Zhang, Flying plasmonic lens in the near field for high-speed nanolithography, Nat. Nanotechnol. 3 (2008) 733–737.
- [29] L. Liu, K. Zhong, T. Munro, S. Alvarado, R. Côte, S. Creten, E. Fron, H. Ban, M. Van der Auweraer, N.B. Roozen, O. Matsuda, C. Glorieux, Wideband fluorescence-based thermometry by neural network recognition: photothermal application with 10 ns time resolution, J. Appl. Phys. 118 (2015) 184906.
- [30] U.N. Gaitonde, D.D. Deshpande, S.P. Sukhatme, The thermal conductivity of liquid mixtures, Ind. Eng. Chem. Fund. 17 (1978) 321–325.